Electrochimica Acta 283 (2018) 1231–1237

Contents lists available at ScienceDirect

Electrochimica Acta

journal homepage: www.elsevier.com/locate/electacta

# Engineering surface states and band edge of $TiO_2$ microspheres by tuning pH value of hydrothermal treatment

Chun Gao [a, b], You-Cai Ding [a, b], Li-E Mo [a], Zhao-Qian Li [a], Xiao-Qiang Shi [e], Lin-Hua Hu [a, *], Tasawar Hayat [c, d], Ahmed Alsaedi [c], Song-Yuan Dai [a, e, **]

[a] Key Laboratory of Photovoltaic and Energy Conservation Materials, Institute of Applied Technology, Hefei Institutes of Physical Science, Chinese Academy of Sciences, Hefei, 230031, PR China
[b] University of Science and Technology of China, Hefei, 230026, PR China
[c] NAAM Research Group, Department of Mathematics, Faculty of Science, King Abdulaziz University, Jeddah, 21589, Saudi Arabia
[d] Department of Mathematics, Quaid-I-Azam University, Islamabad, 44000, Pakistan
[e] Beijing Key Laboratory of Novel Thin Film Solar Cells, North China Electric Power University, Beijing, 102206, PR China

ARTICLE INFO

*Article history:*
Received 17 April 2018
Received in revised form
26 June 2018
Accepted 30 June 2018
Available online 4 July 2018

*Keywords:*
$TiO_2$ microspheres
Surface states
pH values
Charge transfer

ABSTRACT

Herein, $TiO_2$ microspheres were synthesized at different pH values. The effects of pH values on surface states and charge transport performances were investigated. It is noted that alkaline environment leads to a negative band edge of $TiO_2$ microsphere and promotes the interfacial charge transfer. Meanwhile, the charge recombination in the $TiO_2$ microspheres was effectively suppressed in alkaline environment. Besides, $TiO_2$ microspheres synthesized in alkaline condition contained less surface states, which is beneficial to a higher charge collection efficiency and longer diffusion length in dye sensitized solar cells (DSSCs). Moreover, a better crystallinity of $TiO_2$ microspheres can be obtained in an alkaline environment. As a result, when these $TiO_2$ microspheres were used in DSSCs, the device with the $TiO_2$ synthesized at pH = 8 showed the highest performance than that of the device based on $TiO_2$ synthesized in lower pH values.



## 1. Introduction

$TiO_2$, as a promising photoelectric material, is widely employed in solar cells, water splitting, gas sensor, lithium storage, and photocatalysis due to its proper band gap, great photochemical stability and lower prices [1–5]. Particularly, $TiO_2$ microsphere has attracted a lot of attentions and became one of the most crucial photoelectric materials owing to its large surface area, excellent electron transportation performance and prominent scattering effect [6–8]. Compared to commercial $TiO_2$ paste, $TiO_2$ microsphere have several advantages, such as superior light-scattering effect, greater specific surface area and pore size for more dye uptake of the $TiO_2$ microspheres and easy transport of solid electrolyte through mesopores [9]. The efficiency of some DSSCs based on only $TiO_2$ microspheres has been beyond 10.5% if using efficient dye (C 101) and suitable electrolyte (less viscous acetonitrile-based electrolyte) [1,10,11]. Meanwhile, the mechanism of the electron behavior in the material is one of the key issues for the high performance. However, the mechanism of the electron behavior in the material is not clear till now. Numerous surface states exist in $TiO_2$ as a result of great number of defects, such as $Ti^{3+}$ and oxygen vacancy, subsequently resulting in worse electron transfer in $TiO_2$ microsphere [12], which is detrimental to device performance. Studying the surface states and electron transportation process of $TiO_2$ microsphere is helpful to understanding the working mechanism in photoelectric devices [13,14]. J. Biaquert and co-workers found that the electrons in the surface states were distributed in the form of exponential distribution, and the electron concentration in the surface states was much higher than that of the semiconductor conduction band [15]. Cyclic voltammetry (CV) method was used to study light and temperature dependence of surface states in the $TiO_2$ thin film by M. Grätzel. It is found that light can impel the surface states electron to move to a deep level, leading to

* Corresponding author. Key Laboratory of Photovoltaic and Energy Conservation Materials, Institute of Applied Technology, Hefei Institutes of Physical Science, Chinese Academy of Sciences, Hefei, 230031, PR China.
** Corresponding author. Beijing Key Laboratory of Novel Thin Film Solar Cells, North China Electric Power University, Beijing, 102206, PR China.
*E-mail addresses:* lhhu@rntek.cas.cn (L.-H. Hu), sydai@ncepu.edu.cn (S.-Y. Dai).

https://doi.org/10.1016/j.electacta.2018.06.204
0013-4686/

decrease Fermi level [16]. Songyuan Dai et al. reported that the surface states density of $TiO_2$ microspheres was lower than that of $TiO_2$ nanoparticles, resulting in enhanced performance of dye sensitized solar cells (DSSCs) [14]. Although the efficiency was improved obviously by applying microspheres as photoanode in DSSCs, the surface states of $TiO_2$ microspheres still need to be investigated in details.

Herein, a series of $TiO_2$ microspheres were synthesized by a two-step method to explore the influence of pH values on surface states. Since the pH value of hydrothermal condition lower than 5 would affect the crystallization of the $TiO_2$ microspheres and $TiO_2$ microspheres synthesized beyond pH 8 fractured resulting weaker charge transport [13], the pH values were tuned to pH = 5, 6, 7, 8 with different amount of acetic acid and ammonia in the second step. The electron transport behavior, density and distribution of surface states and the band edge shifts in $TiO_2$ microsphere were investigated. The results showed that the density of surface states (DOS) decreased with the rising of pH values in $TiO_2$ microsphere. When applied to DSSCs, the power conversion efficiencies (PCE) of the devices increased with the rising of pH values. Our work also explains the influence of surface states on electron behavior of transport and recombination in the $TiO_2$ films. This work makes a fundamental contribution to a better understanding of the working mechanism in DSSCs.

## 2. Experimental section

### 2.1. Synthesis of $TiO_2$ microspheres

All the Chemical reagents were purchased from Sigma-Aldrich and used without further purification. The $TiO_2$ microspheres were prepared firstly by a sol-gel process of TTIP (Titanium(IV) isopropoxide) hydrolysis to prepare amorphous microspheres and followed a hydrothermal treatment. The different pH values of hydrothermal reaction were controlled by adding different volumes of ethylic acid or ammonia to the solution. The typical synthesis process was as follows: 500 mL of ethanol, 1.4 mL of deionized water and 1.4 mL of KI solution were mixed to form a homogeneous solution, 12 mL of TTIP was dropwise added into the homogeneous solution followed by magnetic stirring for 24 h to form a milky white suspension by the process of TTIP hydrolysis. Subsequently, the precipitates were collected by centrifugation and washed several times with ethanol, followed by drying in 30 °C for 1 h. Then, the obtained products were dispersed in a mixture of 40 mL ethanol and 20 mL $H_2O$. Different volumes of ethylic acid or ammonia were added to the solution to tune the pH values. Afterwards, the mixtures were transferred into a Teflon-lined stainless autoclave with a capacity of 100 mL and kept in an oven at 160 °C for 16 h. Finally, the products were washed for several times with ethanol and deionized water alternately, followed drying for characterization. For simplicity, Samples prepared in pH = 5, 6, 7, 8 were denoted as P-5, P-6, P-7, P-8, respectively.

### 2.2. DSSCs fabrication

The as-prepared products were mixed with ethanol, ethyl cellulose and α-terpineol to form four different pastes. The four pastes followed by a screen printing process were printed onto the FTO glass (15 Ω $sq^{-1}$). After sintered in air at 510 °C for 30 min. The film thicknesses were acquired by a profilometer (XP-2, AMBIOS Technology Inc., USA). Then, these four films were immersed into a C101 dye solution ($3 \times 10^{-4}$ M) with cheno-3a, 7a-dihydroxy-5b-cholic acid for 12 h. After being washed by acetonitrile and dried, the films were assembled with a Pt-modified counter electrode by a laser engraved 60 μm Surlyn gasket under heat and pressure. Electrolyte solution (50 mM LiI, 30 mM $I_2$, 1 M 1,3-dimethylimidazolium iodide (DMII), 0.5 M tertbutylpyridine, and 0.1 M guanidinium thiocyanate (GuSCN) in a solvent mixture of 15% valeronitrile with 85% acetonitrile) was introduced into the space between the counter electrode and photoanodes [1].

### 2.3. Characterization

The morphologies of $TiO_2$ samples were observed by a scanning electron microscopy (SEM) (S-4800, HITACHI, Japan). The XRD data of the prepared samples were collected in a 2θ range from 10° to 70° on a X ray diffractometer (MXPAHF, Mark Corp., Japan) with a Cu Kα1 radiation (k = 0.154056 nm) at room temperature. The grain sizes of the materials were analyzed Scherrer equation according to the XRD data. The surface areas of the materials were estimated via the Brunauer–Emmett–Teller (BET) method. Cyclic voltammetry curves were measured by a standard three-electrode cell (using prepared films as the working electrode, a Hg/HgCl (0.1 M $LiClO_4$) as reference electrode and a Pt wire as counter electrode) to study the surface states of $TiO_2$ microspheres. A computer controlled potentiostat (Autolab 320, Metrohm, Switzerland) in a frequency range of 10 mHz–1 MHz applied in the dark was applied to record the Electrochemical Impedance Spectra (EIS) data. Intensity-modulated photocurrent/photovoltage spectroscopy (IMPS/IMVS) was measured on IM6e workstation using light-emitting diodes (λ = 610 nm) driven by Xpot (Germany, Zahner). The current density–voltage curves were measured by a Keithley model 2420 digital source meter controlled by Test point software under a xenon lamp (100 mW $cm^{-2}$).

## 3. Result and discussion

### 3.1. Characterization

The morphology of the $TiO_2$ microspheres are shown in Fig. 1. Obviously, all the $TiO_2$ microspheres have a smooth surface and the crystal grains of P-5, P-6, P-7 are similar. Nevertheless, the grain size of P-8 is obviously larger than other $TiO_2$ microspheres, indicating the nucleation of $TiO_2$ would decrease in the alkaline environment. Fig. S1a shows the XRD patterns of the four samples, all the peaks being in accordance with the pure anatase $TiO_2$ (JCPDS NO.21-1272). The sizes of the crystals were calculated by Scherrer equation [1] based on the (101) peaks (Fig. S1b). The results showed the crystal sizes of P-5, P-6, P-7, P-8 are 15.22, 17.93, 21.24, 22.81 nm, respectively. $N_2$ adsorption/desorption curves of $TiO_2$ microspheres were shown in Fig. S1c, and the average surface areas of P-5, P-6, P-7, P-8 are 100.02, 78.07, 67.25, 53.30 $m^2g^{-1}$ respectively. The surface areas decreased as the raising of pH value, which is ascribed to the raising of crystal sizes of $TiO_2$ microspheres.

### 3.2. Number of surface states

The energy level distribution and total number of surface states in the $TiO_2$ electrodes were characterized in terms of CV measurements [17,18]. The samples were stabilized at −1.2 V for 20 min and the potential was scanned to 0.8 V (The scanning rate is 500 mV $s^{-1}$). As Shown in Fig. 2a, four curves of different $TiO_2$ films exhibit similar shapes. There is a peak in every CV curve at about −0.7 V to −0.5 V in every CV curve, which is attributed to the surface states in the forbidden band. In equilibrium, the surface states would trap numerous Photo-induced electrons. The current peak was generated by introducing of surface states electrons to the conduction band. The detailed process was as follows: Applying an increasing negative potential, the quasi-Fermi level would move to the conduction band. The electrons trapped by surface states would

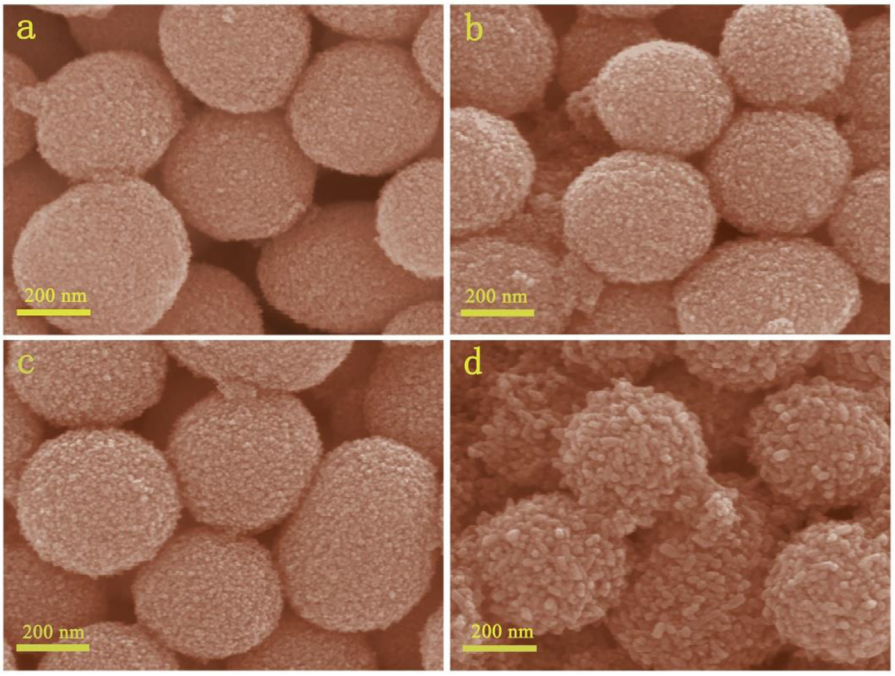


**Fig. 1.** SEM images of $TiO_2$ microspheres. (a) P-5, (b) P-6, (c) P-7, (d) P-8.

be injected to the conduction band when the quasi-Fermi level touch the edge of the conduction band, leading to the increasing of capacitive current. The potential value means the distance quasi-Fermi level moved to the conduction band under the bias potential. When the potential increased positively, the current was closed to zero, indicating the recovery of the injected negative charge and regeneration of most surface states [14,18]. In that way, larger number of surface states would supply more trapped electrons to the conduction band thus resulting higher capacitive current. In addition, energy level distribution could be calculated by the following equations according to the CV measurements [19]:

$$\frac{dQ}{dV} = DOS\frac{N_A}{F} \quad (1)$$

$$dQ = \frac{1}{v}I(V)dV \quad (2)$$

where $Q$ is the total injected charge, $V$ is the potential applied on the $TiO_2$ photoelectrode, DOS is the density of surface states, $N_A$ is the Avogadro constant, $F$ is Faraday's constant, $I(V)$ is the capacitive current, $v$ represents the constant scanning rate in the cyclic voltammetry. It is worth mentioning that the peak current boosted linearly with the increasing of scanning rate [13]. Hence, the scanning rate must be similar in every measurement. The value of current influenced by scan rates as mentioned above can be given as follows [14,18]:

$$I = I_i + I_c\frac{dQ}{dt} = Cv \quad (3)$$

where $I_c$ is the capacitive current, the $I_i$ is the Faradic current, $v$ is the scanning rate, which can be given by $v = dV/dt$, $C$ is the capacity of the film.

Shown in Fig. 2a, positions of anodic peaks are different, which is related to the potential corresponding to the onset that producing capacitive current. The peak shift with the potential of onset. Moreover, the lower potential of onset means downward shift of the band edge [19], which is similar to the result of Fig. 2b.

Typically, the currents of some samples were not close to zero because of the existence of current induced by electrochemical double layer capacitance (EDLC). From Fig. 2a, four curves of different $TiO_2$ films exhibit similar shapes. According to the results, The EDLC currents of P-5, P-6, P-7, P-8 are about 0.077 mA, 0.044 mA, 0.068 mA, 0.012 mA. After deducting the EDLC current, the rest surface state capacitive current of P-5, P-6, P-7, P-8 is about 1.053 mA, 0.846 mA, 0.702 mA, 0.358 mA at −0.68 V, −0.53 V, −0.73 V, −0.79 V, suggesting that the fewest surface states exist in P-8. The existed surface states in the film would affect the transportation of electrons in the $TiO_2$ network. The lowest voltage (−0.53 V) of P-6 may attribute to the band edge shift of P-6. As the relationship between $V_{oc}$ and ln ($Q$) shows, the band edge of P-6 shifted most positively. Thus, lowest bias would lead the quasi-Fermi level touch the conduction band causing the current increasing. Besides, the EDLC current of P-7 is larger than that of P-6 but the specific surface area of P-7 is smaller than that of P-6, which may ascribe that some micropores make contributions to the specific surface area but make no contributions to EDLC because of few charges adsorbed on that micropores.

### 3.3. Photo induced electron density and band edge shifts

Information related to photo induced electron density ($Q$) in DSSCs can be acquired in terms of IMPS/IMVS measurements [20,21]. IMPS/IMVS is a frequency-resolved measurement that sine modulated light is applied to study semiconductor electrode system. $TiO_2$ photoanode was irradiated by monochromatic incident light. The incident light consists of direct current background and modulated light intensity. In short circuit, the IMPS provided the dynamic information of charge transfer inside the electrode, and the charge transfer time can be obtained [22]. In the case of open circuit, the electron lifetime ($\tau_n$) can be measured with IMVS [23]. Two experimental methods are used to understand the carrier

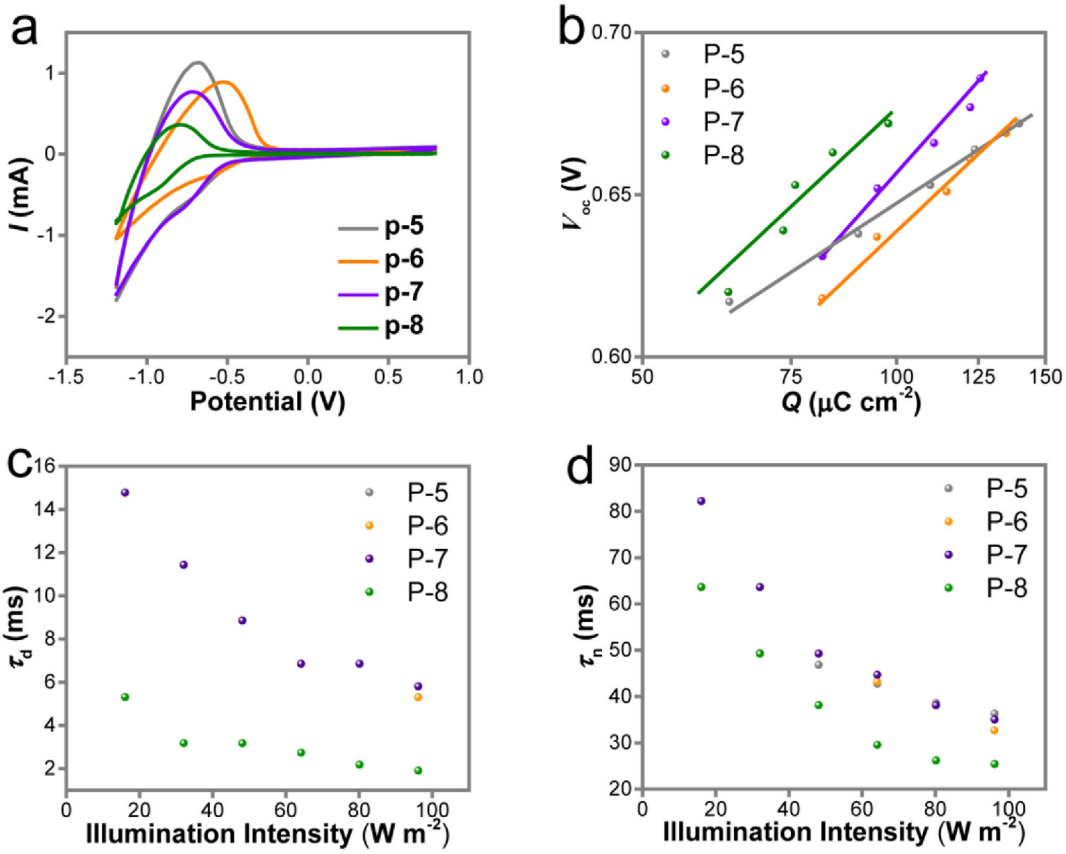


**Fig. 2.** (a) Cyclic voltammograms of four $TiO_2$ films at a scan rate of 500 mV $s^{-1}$. (b) $V_{oc}$ as a function of ln Q for the four samples. (c) Electron transport time and (d) electron lifetime as a function of illumination intensity for the four DSSCs. (The missing points in (c) and (d) were overlapped).

transport and complex process in dye-sensitized solar cells. Moreover, the different $V_{oc}$ and $J_{sc}$ can be obtained under different intensity of incident light. The photo-induced charge can be calculated by $Q = J_{sc} \cdot \tau_n$. Thus, the relationship between $V_{oc}$ and ln (*Q*) can be obtained from the IMPS/IMVS measurements [24]. According to the IMPS/IMVS results, the relationship between $V_{oc}$ and ln (*Q*) is shown in Fig. 2b. As Seen in Fig. 2b, the relationship between $V_{oc}$ and ln (*Q*) is approximatively linear, which can be fitted by the following equation [20,21]:

$$V_{oc} + V_c + m_c \ln(Q) \quad (4)$$

where $m_c$ is a constant coefficient and the $V_c$ is value when ln $(Q) = 0$. The electrons recombination behavior can be valued from the $m_c$. It was proposed previously that the electrons recombination would happen by the surface states if the $m_c > 26$ mV. Otherwise, it would happen via the conduction band [25]. The $m_c$ value of the four films were 75.84 mV, 93.49 mV, 103.47 mV and 105.85 mV, suggesting that electrons recombination was via surface states. It is worth noting that when the value of $V_{oc}$ is the same, the values of required *Q* varied wildly. According to Fig. 2b, P-6 possessed the maximum numbers of *Q* in the same $V_{oc}$, which helps to give a larger $J_{sc}$. As Table 2 shows, the $J_{sc}$ of P-6 is larger than others, which is consistent with the above results. Typically, the discrepancy between the bottom of the conduction band and the electrons quasi-Fermi level were decided by the accumulated charges, supposing that the accumulated charges would affect the shifts of the band edges [21,25]. The band edge shifts can be seen in Fig. 2b. For the same *Q*, the decreasing $V_{oc}$ indicates the positive shifts of the band edge [25]. Accordingly, a lower $V_{oc}$ might be obtained in P-5 and P-6, which is in parallel with the results in Table 2. Typically, shown in Table 1, the $V_{oc}$ of four samples are all over 0.7 V, which means that the required *Q* for the four samples is over 100 μC $cm^{-2}$. In this case, the decreasing $V_{oc}$ order of the four samples should be P-8 > P-7 > P-6 > P5. Actually, the $V_{oc}$ order of the four samples is P-8 > P-7 > P-5 > P6. The reason for the $V_{oc}$ of P-5 is bigger than that of P-6 might be that the capacitance of P-5 is bigger that of P-6, providing more *Q* to improve $V_{oc}$ of P-5.

### 3.4. The electron transport and recombination

According to random walk model [26], the electron would stay in a surface state decided by the active energy for a while before transport. The transport of electrons in the $TiO_2$ microspheres was affected by trapping and detrapping process significantly [26,27]. The existing of the surface states was ascribed to the imperfection in the boundary of the crystal and internal defects. Furthermore, the deficiency of the cation also caused a lot of surface states in the forbidden band [12]. The electron transport time ($\tau_d$) and lifetime ($\tau_n$) are affected by surface states in the $TiO_2$ microspheres. Here $\tau_d$ is the time spent in the process that from electrons injection

**Table 1**
Characteristic parameters of the EIS spectra of four DSSCs in the dark at −0.75 V.

| Cell | $R_{ct}$ (Ω) | CPE2 (mF) | $\tau$ (ms) |
|---|---|---|---|
| P-5 | 25.2 | 2.26 | 57.0 |
| P-6 | 27.7 | 2.01 | 55.7 |
| P-7 | 19.44 | 2.27 | 44.1 |
| P-8 | 30.8 | 0.986 | 30.4 |

**Table 2**
Photovoltaic characteristic of the four DSSCs.

| Cell | $J_{sc}$ (mA cm$^{-2}$) | $V_{oc}$ (V) | FF | PCE |
|---|---|---|---|---|
| P-5 | 16.28 | 0.709 | 0.733 | 8.46 |
| P-6 | 18.70 | 0.708 | 0.733 | 9.71 |
| P-7 | 18.44 | 0.723 | 0.738 | 9.84 |
| P-8 | 18.67 | 0.724 | 0.765 | 10.34 |

towards conduction band to electrons collection in the substrate. Meanwhile, $\tau_n$ is the time spent between the generation of photo induced electrons and the recombination of electron and I- 3 in the electrolyte. The $\tau_d$ and $\tau_n$ results were derived from IMPS/IMVS measurements [28,29]. Shown in Fig. 2c and d. The value of $\tau_d$ and $\tau_n$ were calculated by the expressions: $\tau_d = 1/2\pi f_{IMPS}$, $\tau_n = 1/2\pi f_{IMVS}$, where the $f_{IMPS}$ and $f_{IMVS}$ are the characteristic frequency of the IMPV/IMVS imaginary component [30]. The result shows that $\tau_d$ and $\tau_n$ are both decreasing with the increasing of the illumination intensity. With the raising of illumination intensity, electrons in the deep energy levels are stimulated to the shallow energy levels, leading to quasi-Fermi levels shift to the conduction band. Hence, more electrons exist in the shallow energy levels, thus beneficial to a fast transport speed [25]. For the decreasing of $\tau_n$, in terms of the same reason, less electrons are trapped in the deep energy trap states, leading larger recombination rate with I- 3. As a result, the $\tau_n$ shifts to a lower value. Seen in Fig. 2c, P-8 shows a smaller $\tau_d$ when compared to other samples under the same light intensity level, indicating that electron inside P-8 transported more quickly than others.

However, the electron lifetime of P-8 is also the smallest in the four photoelectrodes. To assess the competition between electron transport and electron recombination, the charge collection efficiency ($\eta_{coll}$) was proposed to characterize the performances of DSSCs, which can be obtained by the equation [31,32]:

$$\eta_{coll} = 1 - \tau_d/\tau_n \quad (5)$$

A larger $\eta_{coll}$ indicates a better property of the DSSCs. Fig. 3a shows the charge collection efficiency of DSSCs based on four photoelectrodes. As a consequence, $\eta_{coll}$ value of P-8 is larger than that of other samples, indicating a better performance in P-8. It can be concluded that less deep surface states exit in P-8 as compared with other photoelectrodes.

Besides, When the film thickness is taken into consideration, electron diffusion length ($L_n$) is also a significant quantity to characterize the performance of the DSSCs, which can be expressed by the following equation [33]:

$$L_n = (D_n\tau_n)^{1/2} \quad (6)$$

where $D_n$ is the diffusion coefficient decided by the thickness ($d$) of the film and $\tau_d$, which can be expressed by the following equation [22]:

$$D_n = d^2/(2.35\tau_d) \quad (7)$$

Fig. 3b shows the diffusion length as a function of illumination intensity for the DSSCs based on four samples. The diffusion length of DSSCs based on P-8 is larger than other samples, indicating a better performance of charge transport [34]. The results demonstrate that the diffusion of electrons of DSSCs based on P-8 $TiO_2$ microsphere is more efficient than that of other cells, which may be attributed to the higher crystallinity of P-8 $TiO_2$ microsphere in terms of the SEM (Fig. 1) and the XRD results in the supporting information (Table S1).

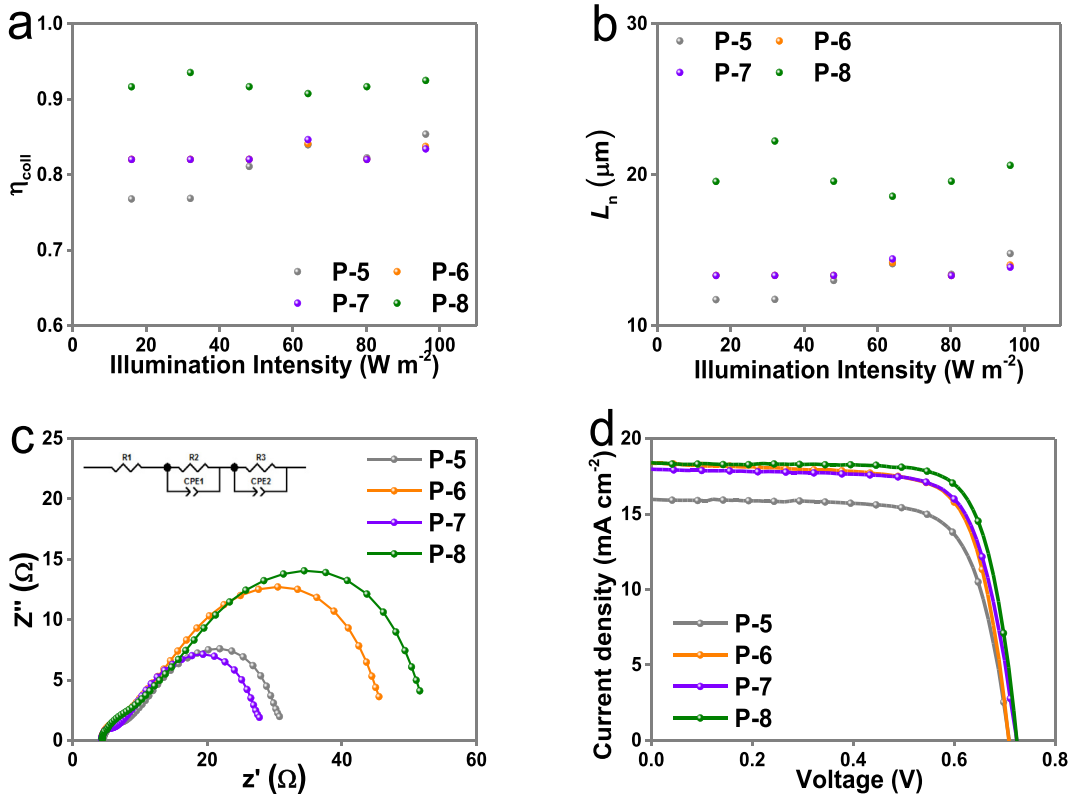


**Fig. 3.** (a) Charge collection efficiency and (b) Electron diffusion length as a function of the illumination intensity for different photoanodes. (c) Nyquist plots of the four DSSCs at a forward bias of −0.75 V in the dark. (d) *J-V* curves of the DSSCs with the four photoanodes. (The missing points in (c) and (d) were overlapped).

### 3.5. Kinetics process of the interface

Electrochemical impedance spectroscopy (EIS) is a powerful characterization to give information about electrochemical behavior within DSSCs. DSSCs based on four $TiO_2$ microsphere were measured in the dark environment at different potential. Fig. 3c is the Nyquist plots of DSSCs based on four $TiO_2$ photoanodes characterized at −0.75 V. The corresponding equivalent circuit of device is displayed in the inset. Seen in the Fig. 3c, two hemispheres can be recognized at every curve, revealing the charge transfer at the interface of Pt counter electrode/electrolyte and $TiO_2$/dye/electrolyte [35]. Large hemisphere at the low frequency indicates the electrochemical reaction on photoanode/electrolyte interface and small hemisphere at the high frequency reflects the kinetics process on Pt cathode. Since the same Pt counter electrodes were employed in each device, the smaller hemisphere exhibits similarly. As a result of the difference of $TiO_2$ photoanodes between every DSSCs, the hemispheres at the high frequency region varied widely. According to this method, some significant data can be acquired by fitting the results. The fitted results were summarized in Table 1.

As shown in Table 1, the recombination resistance ($R_{ct}$) of DSSCs decreased significantly from 30.8 Ω to 25.2 Ω with the decreased pH value from 8 to 5 (except P-7), indicating a larger recombination rate occurred within DSSCs based on the $TiO_2$ microsphere with decreased pH and the most severe electron recombination process in the DSSCs based on the P-5 microsphere which possessed numerous surface states. Typically, the $R_{ct}$ of P-7 is smallest but the DOS is not the biggest in all the candidates, which may ascribe to more numerous grain boundaries. Moreover, since the $V_{oc}$ value of the DSSCs was correlated with the charge recombination in the conduction band of $TiO_2$, the $V_{oc}$ of P-8 is highest owing to the largest $R_{ct}$. However, P-7 has low $R_{ct}$ but high $V_{oc}$, which may ascribe to the larger chemical capacitance (CPE2) of P-7 providing more charge to acquire higher $V_{oc}$. Same conclusion can be deduced from the literature [36]. Besides, the electron lifetimes ($\tau_{n(EIS)}$) are also up to the value of chemical capacitance (CPE2), which can be acquired in terms of the equation: $\tau_{n(EIS)} = R_{ct} \times CPE2$ [37]. Seen in Table 1, the $\tau_{n(EIS)}$ of P-5, P-6, P-7, P-8 DSSCs are 57.0, 55.7, 44.1, 30.4 ms respectively, which is similar with the IMPS/IMVS results in Fig. 2d.

### 3.6. DSSCs performances

DSSCs fabrication has been introduced in the experiment section. Four kinds of DSSCs based on different $TiO_2$ microspheres were measured by a Keithley model 2420 digital source meter controlled by Test point software under a xenon lamp (100 mW $cm^{-2}$). *J-V* curves are shown in Fig. 3d with the parameters listed in Table 2. As Table 2 shows, the PCE raised as the pH value increased. P-6 shows the highest $J_{sc}$ and P-8 shows the highest $V_{oc}$, which can be explained by the results of the band edge movements and collection efficiency of electrons. Compared to P-7, P-5 and P-6 had a positive movements of band edge resulting in a lower $V_{oc}$. While P-8 had negative band edge movements thus beneficial to a higher $V_{oc}$. Otherwise, because of the raising of charge collection efficiency with the increasing of pH, the PCE showed a raising tendency.

## 4. Conclusions

In summary, the $TiO_2$ microsphere was synthesized in different pH values and the charge transport performances was further investigated. According to the results, less surface states exit in $TiO_2$ microsphere synthesized in pH = 8. Meanwhile, when pH value exceeds 7, a negative band edge shift would be caused, which gave rise to a higher $V_{oc}$ in DSSCs based on P-8. EIS measurements revealed that both acidic and alkaline environment would increase the recombination resistances and lower chemical capacitance of the films. Moreover, the crystallization was also influenced by the pH values. Alkaline environment would cause a better crystallinity as exhibited in the results of SEM and XRD. In addition, the higher collection efficiency and longer diffusion length attributed to a higher $J_{sc}$ in P-8 according to the IMVS/IMPS results. Thus, DSSCs with higher photoelectric conversion efficiencies are realized based on P-8 $TiO_2$ microspheres. We believe that such an investigation is significative to develop $TiO_2$ with less surface states and make contributions to design promising candidates in various areas such as DSSCs, sensors, photoelectrochemical water splitting, batteries and photocatalysis. To achieve $TiO_2$ with more remarkable properties, further researches about the mechanism of charge behavior in $TiO_2$ microspheres are still necessary.

## Acknowledgments

This work was supported by the National High Technology Research and Development Program of China (No. 2015AA050602), the External Cooperation Program of BIC, Chinese Academy of Sciences under Grant No. GJHZ1607, and the Major/Innovative Program of Development Foundation of Hefei Center for Physical Science and Technology (2016FXZY003).

## Appendix A. Supplementary data

Supplementary data related to this article can be found at https://doi.org/10.1016/j.electacta.2018.06.204.

## References

[1] Y. Ding, L. Zhou, L.E. Mo, L. Jiang, L. Hu, Z. Li, S. Chen, S. Dai, $TiO_2$ microspheres with controllable surface area and porosity for enhanced light harvesting and electrolyte diffusion in dye-sensitized solar cells, Adv. Funct. Mater. 25 (2015) 5946–5953.
[2] J. Zhang, X. Jin, P.I. Moralesguzman, X. Yu, H. Liu, H. Zhang, L. Razzari, J.P. Claverie, Engineering the absorption and field enhancement properties of Au-$TiO_2$ nanohybrids via whispering gallery mode resonances for photocatalytic water splitting, ACS Nano 10 (2016) 4496.
[3] M. Zhang, T. Xue, S. Xu, Z. Li, Y. Yan, Y. Huang, Adverse effect of substrate surface impurities on $O_2$ sensing properties of $TiO_2$ gas sensor operating at high temperature, Ceram. Int. 43 (2017) 5842–5846.
[4] X.Y. Yu, H.B. Wu, L. Yu, F.X. Ma, X.W. Lou, Rutile $TiO_2$ submicroboxes with superior lithium storage properties, Angew. Chem. Int. Ed. 54 (2015) 4001–4004.
[5] H. Park, H. Kim, G. Moon, W. Choi, Photoinduced charge transfer processes in solar photocatalysis based on modified $TiO_2$, Energy Environ. Sci. 9 (2016) 411–433.
[6] J. Du, J. Qi, D. Wang, Z. Tang, Facile synthesis of Au@ $TiO_2$ core–shell hollow spheres for dye-sensitized solar cells with remarkably improved efficiency, Energy Environ. Sci. 5 (2012) 6914–6918.
[7] J. Ferber, J. Luther, Computer simulations of light scattering and absorption in dye-sensitized solar cells, Sol. Energy Mater. Sol. Cells 54 (1998) 265–275.
[8] X. Lai, J.E. Halpert, D. Wang, Recent advances in micro-/nano-structured hollow spheres for energy applications: from simple to complex systems, Energy Environ. Sci. 5 (2012), 9944-9944.
[9] H.G. Jung, S. Nagarajan, Y.S. Kang, Y.K. Sun, Nanostructured $TiO_2$, microspheres for dye-sensitized solar cells employing a solid state polymer electrolyte, Electrochim. Acta 89 (2013) 848–853.
[10] Y. Ding, X. Xia, W. Chen, L. Hu, L.E. Mo, Y. Huang, S. Dai, Inside-out Ostwald ripening: a facile process towards synthesizing anatase $TiO_2$ microspheres for high-efficiency dye-sensitized solar cells, Nano Res. 9 (2016) 1891–1903.
[11] L. Heiniger, F. Giordano, T. Moehl, M. Grätzel, Mesoporous $TiO_2$ beads offer improved mass transport for cobalt-based redox couples leading to high efficiency dye-sensitized solar cells, Adv. Energy Mater. 4 (12) (2015) 1400168 (2014).
[12] S.H. Kang, J.-Y. Kim, Y.-E. Sung, Role of surface state on the electron flow in modified $TiO_2$ film incorporating carbon powder for a dye-sensitized solar cell, Electrochim. Acta 52 (2007) 5242–5250.
[13] J. Zheng, L. Mo, W. Chen, L. Jiang, Y. Ding, Z. Li, L. Hu, S. Dai, Surface states in $TiO_2$ submicrosphere films and their effect on electron transport, Nano Res. 10 (2017) 3671–3679.
[14] J. Zheng, L. Mo, W. Chen, L. Jiang, Y. Ding, Y. Ding, Z. Li, L. Hu, S. Dai, An investigation of surface states energy distribution and band edge shifts in solar cells based on $TiO_2$ submicrospheres and nanoparticles, Electrochim.

Acta 232 (2017) 38–43.
[15] J. Bisquert, F. Fabregat-Santiago, I. Mora-Seró, G. Garcia-Belmonte, E.M. Barea, E. Palomares, A review of recent results on electrochemical determination of the density of electronic states of nanostructured metal-oxide semiconductors and organic hole conductors, Inorg. Chim. Acta 361 (2008) 684–698.
[16] Qing Wang, Z. Zhang, S.M.Z, M. Grätzel, Enhancement of the performance of dye-sensitized solar cell by formation of shallow transport levels under visible light illumination, J. Phys. Chem. C 112 (2008) 7084–7092.
[17] M. Bailes, P. Cameron, K. Lobato, L. Peter, Determination of the density and energetic distribution of electron traps in dye-sensitized nanocrystalline solar cells, J. Phys. Chem. B 109 (2005) 15429–15435.
[18] N. Duffy, L. Peter, R. Rajapakse, K. Wijayantha, A novel charge extraction method for the study of electron transport and interfacial transfer in dye sensitised nanocrystalline solar cells, Electrochem. Commun. 2 (2000) 658–662.
[19] Z. Zhang, S.M. Zakeeruddin, B.C. O'Regan, R. Humphry-Baker, M. Grätzel, Influence of 4-guanidinobutyric acid as coadsorbent in reducing recombination in dye-sensitized solar cells, J. Phys. Chem. B 109 (2005) 21818–21824.
[20] X. Ren, Q. Feng, G. Zhou, C.-H. Huang, Z.-S. Wang, Effect of cations in coadsorbate on charge recombination and conduction band edge movement in dye-sensitized solar cells, J. Phys. Chem. C 114 (2010) 7190–7195.
[21] G. Schlichthörl, S. Huang, J. Sprague, A. Frank, Band edge movement and recombination kinetics in dye-sensitized nanocrystalline $TiO_2$ solar cells: a study by intensity modulated photovoltage spectroscopy, J. Phys. Chem. B 101 (1997) 8141–8155.
[22] G. Schlichthörl, a.N.G. Park, A.J. Frank, Evaluation of the charge-collection efficiency of dye-sensitized nanocrystalline $TiO_2$ solar cells, J. Phys. Chem. B 103 (5) (1999) 782–791.
[23] Y. Liu, A. Hagfeldt, X.R. Xiao, S.E. Lindquist, Investigation of influence of redox species on the interfacial energetics of a dye-sensitized nanoporous $TiO_2$, solar cell, Sol. Energy Mater. Sol. Cells 55 (3) (1998) 267–281.
[24] K. Zhu, N. Kopidakis, N.R. Neale, J. van De Lagemaat, A.J. Frank, Influence of surface area on charge transport and recombination in dye-sensitized $TiO_2$ solar cells, J. Phys. Chem. B 110 (2006) 25174–25180.
[25] D. Kou, W. Liu, L. Hu, S. Dai, Cooperative effect of adsorbed cations on electron transport and recombination behavior in dye-sensitized solar cells, Electrochim. Acta 100 (2013) 197–202.
[26] J. Nelson, S.A. Haque, D.R. Klug, J.R. Durrant, Trap-limited recombination in dye-sensitized nanocrystalline metal oxide electrodes, Phys. Rev. B 63 (2001) 205321.
[27] J. Van de Lagemaat, N.-G. Park, A. Frank, Influence of electrical potential distribution, charge transport, and recombination on the photopotential and photocurrent conversion efficiency of dye-sensitized nanocrystalline $TiO_2$ solar cells: a study by electrical impedance and optical modulation techniques, J. Phys. Chem. B 104 (2000) 2044–2052.
[28] W. Liu, L. Hu, S. Dai, L. Guo, N. Jiang, D. Kou, The effect of the series resistance in dye-sensitized solar cells explored by electron transport and back reaction using electrical and optical modulation techniques, Electrochim. Acta 55 (2010) 2338–2343.
[29] T. Oekermann, T. Yoshida, H. Minoura, K. Wijayantha, L. Peter, Electron transport and back reaction in electrochemically self-assembled nanoporous ZnO/dye hybrid films, J. Phys. Chem. B 108 (2004) 8364–8370.
[30] H. Wang, P.G. Nicholson, L. Peter, S.M. Zakeeruddin, M. Grätzel, Transport and interfacial transfer of electrons in dye-sensitized solar cells utilizing a Co $(dbbip)_2$ redox shuttle, J. Phys. Chem. C 114 (2010) 14300–14306.
[31] T. Oekermann, D. Zhang, T. Yoshida, H. Minoura, Electron transport and back reaction in nanocrystalline $TiO_2$ films prepared by hydrothermal crystallization, J. Phys. Chem. B 108 (2004) 2227–2235.
[32] K. Zhu, T.B. Vinzant, N.R. Neale, A.J. Frank, Removing structural disorder from oriented $TiO_2$ nanotube arrays: reducing the dimensionality of transport and recombination in dye-sensitized solar cells, Nano Lett. 7 (2007) 3739–3746.
[33] J.R. Jennings, A. Ghicov, L.M. Peter, P. Schmuki, A.B. Walker, Dye-sensitized solar cells based on oriented $TiO_2$ nanotube arrays: transport, trapping, and transfer of electrons, J. Am. Chem. Soc. 130 (2008) 13364–13372.
[34] J.P. Gonzalezvazquez, J.A. Anta, J. Bisquert, Determination of the electron diffusion length in dye-sensitized solar cells by random walk simulation: compensation effects and voltage dependence, J. Phys. Chem. C 114 (2010) 8552–8558.
[35] Francisco Fabregatsantiago, Juan Bisquert, Emilio Palomares, Luis Otero, Daibin Kuang, S.M.Z, Michael Grätzel, Correlation between photovoltaic performance and impedance spectroscopy of dye-sensitized solar cells based on ionic liquids, J. Phys. Chem. C 111 (2007) 6550–6560.
[36] Y.S. Tingare, Nguyễn So'n Vinh, H.H. Chou, Y.C. Liu, Y.S. Long, T.C. Wu, T.C. Wei, C.Y. Yeh, New acetylene-bridged 9,10-conjugated anthracene sensitizers: application in outdoor and indoor dye-sensitized solar cells, Adv. Energy Mater. 7 (18) (2017) 1700032.
[37] D. Kuang, C. Klein, Z. Zhang, S. Ito, J.E. Moser, S.M. Zakeeruddin, M. Grätzel, Stable, high-efficiency ionic-liquid-based mesoscopic dye-sensitized solar cells, Small 3 (2007) 2094.